Partially Filled Nutation Damper for a Freely Precessing Gyroscope

C. O. Chang* and C. S. Chou*
National Taiwan University, Taipei, 10764, Taiwan, Republic of China

Transient responses of a freely precessing gyroscope carrying a partially filled mercury ring damper are analyzed. An eccentric annulus is proposed to model the experimentally observed shape of the mercury, which is considered as deformable continuum. The variables describing the position of the center of mass of this continuum are defined as generalized coordinates. The frictional force between the mercury and the wall of the damper is derived in terms of the variables defining the free surface of the mercury and their time derivatives. Coupled equations of motion of the mercury and the rotor are derived by Lagrange's method in the form of ordinary differential equations rather than partial differential equations. These equations are employed in analyzing the effects of the parameters of the damper on the decay time constant of the nutation angle. The number of rings in the damper and the amount of mercury in each ring both have significant influence on the decay time constant. The theoretically predicted decay time constant is verified by experiment.

Introduction

WHEN a spin-stabilized satellite is subjected to an impulsive torque, i.e., a suddenly applied torque of brief duration, coning motion (or precession) of the spacecraft's spin axis about the angular momentum vector (which is fixed in space in the absence of subsequent external torques) will occur. If the spacecraft contains a ring damper partially filled with mercury and mounted on the rotor, the damper will have the effect of reducing the cone angle (or nutation angle) of free precession so that the spin axis rapidly approaches the angular momentum vector. This concept has been applied in the design of a gyroscopic seeker in a missile to achieve more precise pointing. The effectiveness of the damper depends on the shape of the mercury in the ring. This shape depends mainly on the spin rate of the rotor. At low constant speed, the mercury forms a crescent. At high constant speed, it forms an annulus of uniform thickness and with the inner surface free of contact with the ring. When an impulsive torque is applied to the spinning rotor, it will experience oscillative nutation and precession, which, in turn, will cause periodic motion of the mercury. The behavior of the nutation angle was characterized by three distinct modes, i.e., the nutation synchronous mode, the spin synchronous mode, and the fluid mode. The nutation synchronous mode and spin synchronous mode occur in the case where the mercury remains crescent. The fluid mode occurs in the case where the resulting nutation angle of the rotor is small after being applied a small impulsive torque and the mercury remains annuluslike.

As to the nutation and spin synchronous modes, Cartwright et al.[1] modeled the crescent mercury as a point mass. Alfriend[2] and Alfriend and Spencer[3] modeled it as a rigid slug. The main features of these two modes are that the nutation angle decays drastically in nutation synchronous mode but with small residue in spin synchronous mode. This undesired residual nutation angle is caused by the centrifugal inertia of the unbalance mass of the mercury. Chang and Chou[4] analyzed the effect of parameters of the damper on the decay time constant and the value of residual nutation angle by solving a minimum-time optimization problem.

As to the fluid mode, Bhuta and Koval[5] analyzed the ring damper that was fully filled with viscous fluid and mounted in a plane parallel to the spin axis of a satellite. Carrier and Miles[6] as well as Miles[7] analyzed the ring damper that was partially filled and mounted in a plane perpendicular to the spin axis of the rotor. They adopted the energy-sink approximation to estimate the decay time constant of the nutation angle. The energy-sink approximation assumes that the energy dissipation rate of the fluid equals the rate of kinetic energy change of the rotor. Therefore, it circumvents the need to establish and solve the coupled equations of motion of the rotor and fluid. The decay time constant Miles obtained based on the energy-sink approximation does not agree with the experimental result of Fitzgibbon and Smith.[8]

In the present paper, the equations of motion of the rotor and the mercury for the fluid mode are derived and their interactions are taken into account. The shape of the mercury is approximated by an eccentric annulus and the deformation of the mercury is represented by the movement of the inner free surface of the annulus. We do not consider the motion of each particle of the mercury but the motion of its center of mass in an average sense. This allows the equations of motion of the rotor and the mercury to be obtained by using Lagrange's method in the form of ordinary differential equations rather than partial differential equations. The variables denoting the position of the center of mass of the mercury are defined as generalized coordinates. The treatment of the motion of the mercury like that of a deformable body will lead to the result in which the moments of inertia of the mercury are not constants but functions of generalized coordinates. The analysis of fluid motion is performed to evaluate the shearing forces between the mercury and the wall of the damper. An inviscid flow problem is solved first and then used to form the boundary conditions for the boundary-layer solution. The velocity field of mercury flow inside the boundary layer is obtained in terms of the variables that define the free surface of the mercury.

An experiment was conducted to measure the response of the gyroscope. Good agreement between the theoretical prediction and the experimental result for the decay time constant indicates that our mathematical modeling is valid.

Received Dec. 26, 1989; revision received Sept. 13, 1990; accepted for publication Sept. 13, 1990.

*Associate Professor, Institute of Applied Mechanics.

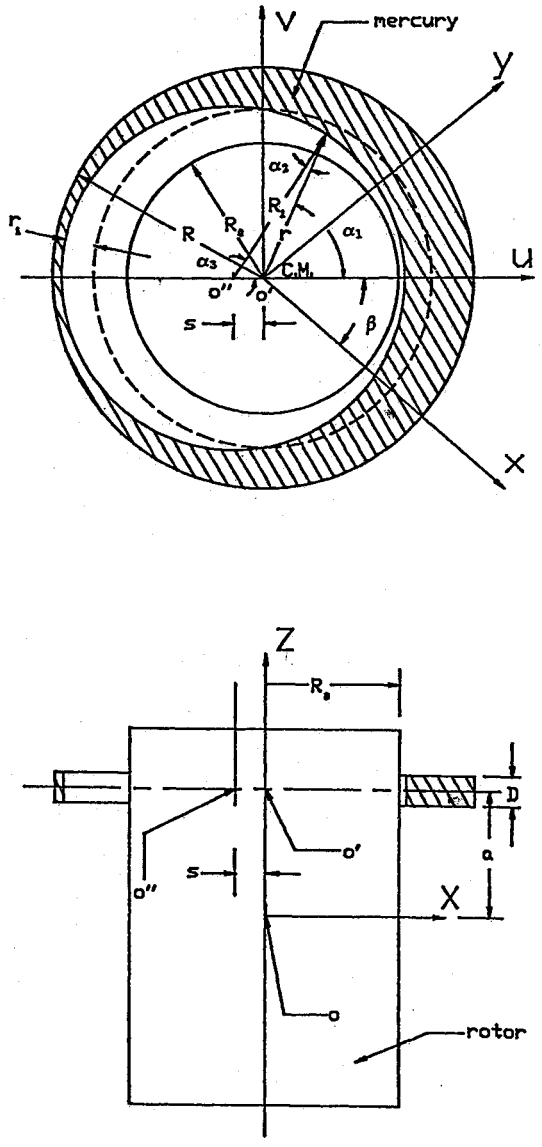

Fig. 1 Idealized model of the mercury filled ring and rotor.

Analysis of Fluid Motion

The rotor of a gyroscopic seeker is made of magnet and connected to the main structure of missiles by a ball joint. The gyroscope is so designed that its center of mass coincides with the center of the ball joint. The spin axis of the rotor is expected to aim at the target. Once the optical detector inside the rotor detects the deviation of the target, the rotor is driven immediately by the impulsive magnetic torque to lock it. The idealized rotor and mercury-filled ring of the gyroscope are shown in Fig. 1. Let a denote the height of the ring damper to the mass center O of the gyroscope, D the thickness of the damper, and R_0 and R the radii of the inner and outer wall of the rectangular cross-section ring, respectively. The angular momentum vector of the gyroscope $\boldsymbol{h}$ about the point O is fixed in space since the system is free after being applied an impulsive torque. The coordinate systems adopted here are shown in Fig. 2. Let the Cartesian coordinate system $OXYZ$ be the inertial reference frame with origin coinciding with the mass center of the gyroscope and the Z axis parallel to $\boldsymbol{h}$. The system $o'xyz$ is fixed on the damper with origin coinciding with the center o' of the ring damper. The orientation of the rotor relative to the $OXYZ$ system is described by a set of three Euler angles. Let ϕ denote the counterclockwise rotation angle about the Z axis of the system x', y', z', which coincides with $OXYZ$ before rotation, θ about the x' axis of the system x'', y'', z'', and ψ about the z'' axis of the system x''', y''', z'''. The x, y, z, axes are parallel to the x''', y''', z''' axes. The $\dot{\phi}$, $\dot{\theta}$, and $\dot{\psi}$ are known as precession, nutation, and spin, respectively. Since for the fluid mode, the nutation angle θ is restricted to be very small, the linearized approximation of $\sin\theta \approx \theta$ and $\cos\theta \approx 1$ will be used in the rest of this section. Because of the small θ assumption, the transformation matrix A from system $o'xyz$ to system $OXYZ$ is[9]

$$A \cong \begin{bmatrix} \cos(\phi+\psi) & \sin(\phi+\psi) & \theta\sin\psi \\ -\sin(\phi+\psi) & \cos(\phi+\psi) & \theta\cos\psi \\ \theta\sin\phi & -\theta\cos\phi & 1 \end{bmatrix} \tag{1}$$

Let r_0 denote the position vector of the point o'. Components of r_0 along the $OXYZ$ axes are

$$r_0 = [a\theta\sin\phi, -a\theta\cos\phi, a]^T \tag{2}$$

Let r_0 denote the position vector of an arbitrary fluid element of the mercury from the point o'. By considering the flow

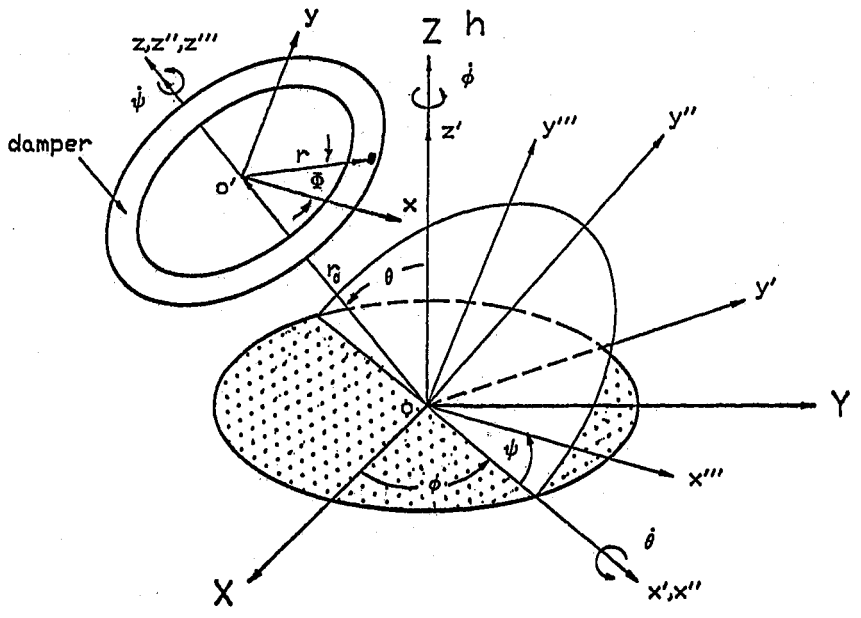

Fig. 2 Coordinate systems.

outside the boundary layer as an inviscid flow, the Euler equations governing this flow relative to the rotor are

$$\frac{Dv}{Dt} + \ddot{r}_0 + \dot{\omega} \times r + \omega \times (\omega \times r) + 2\omega \times v = -\frac{1}{\rho} \nabla p \qquad (3)$$

where v and

$$\frac{Dv}{Dt} = \frac{\partial v}{\partial t} + (v \cdot \nabla)v$$

are the velocity and acceleration of the fluid measured from the x,y,z system, respectively; ω is the angular velocity of the rotor; p the hydrodynamic pressure; and ρ the density of the mercury. Let r,Φ,z denote the cylindrical coordinate system referred to the $o'xyz$ system, $\boldsymbol{B}$ the transformation matrix from system x,y,z to system r,Φ,z. Then the coordinate components of $\ddot{r}_0$ in the r,Φ,z system after some manipulations are given as

$$(\ddot{r}_0)_{r,\Phi,z} = \boldsymbol{B}\boldsymbol{A}^T (\ddot{r}_0)_{X,Y,Z}$$

$$= [a(\ddot{x}_1 \cos\lambda + \ddot{x}_2 \sin\lambda),\ a(\ddot{x}_2 \cos\lambda - \ddot{x}_1 \sin\lambda), 0]^T \qquad (4)$$

where $x_1 = \theta \sin\phi$, $x_2 = -\theta \cos\phi$, and $\lambda = \phi + \psi + \Phi$. Let Ω and $\bar{h}$ denote the spin rate and angular momentum of the gyroscope before it is applied an impulsive torque. This applied impulsive torque is assumed to be small so that the rotor results in motion with small nutation angle and its transverse angular velocities induced are very small in comparison with its spin angular velocity as

$$|\omega_r| \ll \omega_z, \qquad |\omega_\Phi| \ll \omega_z \qquad (5)$$

where ω_r, ω_Φ, and ω_z are coordinate components of ω in the r,Φ,z system. The new angular momentum of the gyroscope $\boldsymbol{h}$ is very close to $\bar{h}$ because of small θ. The mass of the mercury is assumed to be sufficiently smaller than that of the rotor, and so the magnitude of angular momentum of the mercury is neglected in comparison with that of the rotor. From Eq. (5), it is obvious that the magnitude of transverse angular momentum of the rotor is much smaller than that of its spin angular momentum h_r^s. Therefore, we have $\bar{h} \approx h_r^s$, which means that $\omega_z(t) \approx \Omega$. The height of the damper D is assumed to be sufficiently small and the plane of the damper almost remains parallel to the X,Y plane due to small θ, and so the fluid motion can be justified as two-dimensional flow. Substituting Eq. (4) into Eq. (3), using the approximation $\omega = (0,0,\omega_z)^T$, and resolving them into components parallel to r,Φ,z, we obtain

$$\frac{\partial u}{\partial t} + \left(u\frac{\partial u}{\partial r} + \frac{v}{r}\frac{\partial u}{\partial \Phi} - \frac{v^2}{r}\right) + a(\ddot{x}_1 \cos\lambda + \ddot{x}_2 \sin\lambda) - r\omega_z^2 - 2v\omega_z = -\frac{1}{\rho}\frac{\partial p}{\partial r} \qquad (6)$$

$$\frac{\partial v}{\partial t} + \left(u\frac{\partial v}{\partial r} + \frac{v}{r}\frac{\partial v}{\partial \Phi} + \frac{uv}{r}\right) + a(\ddot{x}_2 \cos\lambda - \ddot{x}_1 \sin\lambda) + 2u\omega_z = -\frac{1}{\rho}\frac{1}{r}\frac{\partial p}{\partial \Phi} \qquad (7)$$

where $(r, 0)$ and (u,v) are the coordinate components of r and v along the r,Φ axes. The periodic motion of the mercury flow is induced by the oscillating transverse angular velocity of the rotor, and so the magnitudes of u and v are almost of the same order as that of ω_z. Let the magnitude of u and v be of order U. Then $\partial u/\partial t$ is of order ΩU. In an inviscid flow, $u(\partial u/\partial r)$ is of order U^2, $(v/r)(\partial u/\partial\Phi)$ is of order U^2/R, and v^2/r is of order U^2/R. Since $U^2 \ll \Omega U$, from purely order-of-magnitude considerations, all of those terms in the parentheses of Eqs. (6) and (7) may be neglected. Rearranging the simplified Eqs. (6) and (7) and replacing ω_z by Ω, we obtain

$$\frac{\partial v}{\partial t} + 2\Omega e_z \times v = -\nabla\left[\frac{p}{\rho} - \frac{1}{2}\Omega^2 r^2 + ar(\ddot{x}_1 \cos\lambda + \ddot{x}_2 \sin\lambda)\right] \qquad (8)$$

Taking the curl of Eq. (8) yields $\nabla \times v = 0$; therefore, the flow outside the boundary layer is irrotational flow. The boundary condition is

$$u = 0 \qquad \text{at} \qquad r = R \qquad (9)$$

Let R_1 denote the radius of the inner free surface of the mercury when it forms a concentric annulus. Let $r = R_1 + r_1(\Phi,t)$ be the equation describing the free surface, where r_1 is the amplitude of surface wave. The linearized kinematic boundary condition for the free surface on the assumption of small amplitude waves is

$$u = \frac{\partial r_1}{\partial t} \qquad \text{at} \qquad r = R_1 \qquad (10)$$

The solution of the inviscid irrotational flow that satisfies Eqs. (9) and (10) in terms of the unknown r_1 is

$$\bar{\phi} = \left[\frac{r + (R^2/r)}{1 - (R/R_1)^2}\right]\frac{\partial r_1}{\partial t} \qquad (11)$$

where $\bar{\phi}$ is the velocity potential. Then the velocity field is

$$u = \left[\frac{(R/r)^2 - 1}{(R/R_1)^2 - 1}\right]\frac{\partial r_1(\Phi,t)}{\partial t} \qquad (12a)$$

$$v = -\left[\frac{(R/r)^2 + 1}{(R/R_1)^2 - 1}\right]\frac{\partial^2 r_1(\Phi,t)}{\partial t\,\partial\Phi} \qquad (12b)$$

At the free surface ($r = R_1 + r_1$), the pressure is constant. Linearizing the tangential component of Eq. (8) in r_1 yields

$$\frac{\partial v}{\partial t} + 2\Omega u = \Omega^2\frac{\partial r_1}{\partial t} + Re\{ia\ddot{q}e^{-i\lambda}\} \qquad \text{at} \qquad r = R_1 \qquad (13)$$

where $q = x_1 + ix_2$. The last term in Eq. (13) suggests r_1 in the form

$$r_1(\Phi,t) = aRe\{\zeta(t)e^{-i\lambda}\} \qquad (14)$$

$$\zeta(t) = \xi(t) + i\eta(t) \qquad (15)$$

where ζ and η are the wave variables. The relative displacement between the rotor and the mercury is only along the direction of the shearing force between them, and so the normal force between the mercury and rotor contributes no generalized forces to the Lagrange's equations of the gyroscope. Therefore, we find directly the shearing forces of the viscous flow inside the boundary layer. First we consider the boundary-layer flow over the side wall ($r = R$). The tangential component of momentum Eq. (8) for the inviscid flow is

$$\frac{\partial v}{\partial t} + 2\Omega u = -\frac{1}{r\rho}\frac{\partial p}{\partial \Phi} + Re\{ia\ddot{q}e^{-i\lambda}\} \qquad (16)$$

By modifying Eq. (16), the approximate boundary-layer equation is given as

$$\frac{\partial v'}{\partial t} + 2\Omega u' = -\frac{1}{r\rho}\frac{\partial p'}{\partial \Phi} + Re\{ia\ddot{q}e^{-i\lambda}\} + \nu\frac{\partial^2 v'}{\partial r^2} \qquad (17)$$

where u' and v' are the components of velocity of boundary-layer flow along the r and Φ axes, respectively, and ν is the kinematic viscosity of the mercury. We assume that the radial component of flow velocity u' and the pressure p' in the boundary layer are approximate to those outside the boundary layer. Then the subtraction of Eq. (16) from Eq. (17) yields the simplified momentum equation as

$$\frac{\partial v'}{\partial t} = \frac{\partial v}{\partial t} + \nu \frac{\partial^2 v'}{\partial r^2} \tag{18}$$

The associated boundary conditions are

$$v' = 0, \qquad r = R \tag{19}$$

$$v' = v(R_1,\Phi,t), \qquad \frac{R-r}{\delta} \to \infty \tag{20}$$

where δ is the boundary-layer thickness. By changing variables as $\tau = \Omega t$, $\bar{\eta} = (R-r)/\sqrt{\nu/\Omega}$, and $\hat{v} = v' - v$, the problem of Eqs. (18- 20) becomes

$$\frac{\partial \hat{v}}{\partial \tau} = \frac{\partial^2 \hat{v}}{\partial \bar{\eta}^2} \tag{21}$$

$$\hat{v} = 0, \qquad \bar{\eta} \to \infty \tag{22}$$

$$\hat{v} = -v(R_1,\Phi,\tau), \qquad \bar{\eta} = 0 \tag{23}$$

The problem governed by Eqs. (21-23) is analogous to the Stoke's second problem, that is, the problem of motion of a viscous flow over a flat plate that performs harmonic motion. The transverse angular velocity of a moment-free spinning inertially sysmmetric rotor without damper is harmonic with frequency equal to $(\sigma-1)\Omega$,[5,9] where σ is the ratio of the spin moment of inertia to the transverse moment of inertia of the rotor, and so the wall of the ring is in harmonic motion at the same frequency. With mercury damper added, the frequency of the angular velocity is still very close to $(\sigma-1)\Omega$[7] because the mass and the moment of inertia of the mercury are assumed to be suficiently small in comparison with those of the rotor. In order to assure the frequency of the harmonically moving boundary of Eq. (23) to be $(\sigma-1)\Omega$, the $\zeta(t)$ in Eq. (15) is assumed in the form as

$$\zeta(t) = Qe^{i\sigma\tau}$$

The substitution of Eq. (12b) into Eq. (23) yields

$$\hat{v}(R_1,\Phi,\tau) = D\cos(\sigma-1)\tau + E\sin(\sigma-1)\tau \tag{24}$$

where

$$D = -\left(\frac{R^2+R_1^2}{R^2-R_1^2}\right) a(\sigma-1)\Omega Q\cos\Phi$$

$$E = -\left(\frac{R^2+R_1^2}{R^2-R_1^2}\right) a(\sigma-1)\Omega Q\sin\Phi$$

Note that the Φ in D and E is not an independent variable of Eq. (21). The solution of $\hat{v}$ is immediately available from the standard solution of the Stoke's second problem.
The final solution of v' is

$$v'(r,\Phi,t) = -\left(\frac{R^2+R_1^2}{R^2-R_1^2}\right) ae^{-\chi(R-r)} \times Re\{(\dot{\zeta} - i\Omega\zeta)ie^{-i[\lambda+\chi(R-r)]}\} + \left(\frac{R^2+R_1^2}{R^2-R_1^2}\right) \times aRe\{(\dot{\zeta} - i\Omega\zeta)ie^{-i\lambda}\} \tag{25}$$

where

$$\chi = \sqrt{\frac{(\sigma-1)\Omega}{2\nu}}$$

The shearing force f_s on the side wall in the r,Φ,z system is obtained by integrating the shear stress on the wall as

$$f_s = -\left(\oint \bar{\tau}_{r\Phi}|_{r=R} RDd\Phi\right) e_\Phi \tag{26}$$

Let the coordinate components of f_s along the X,Y axes be (f_X, f_Y, f_Z) and denote $f_1 = f_X + if_Y$. Then by transforming Eq. (26) from r,Φ,z to X,Y,Z we obtain

$$f_1 = -\mu\left(\frac{R^2+R_1^2}{R^2-R_1^2}\right) a\chi DR\pi(\dot{\zeta} - i\Omega\zeta + i\dot{\zeta} + \Omega\zeta) \tag{27}$$

Let $\bar{u}$ and $\bar{v}$ denote the r and Φ coordinate components of velocity of the flow inside the boundary layer of the inner top surface of the ring. The modified momentum equations for this boundary-layer flow are

$$\frac{\partial \bar{u}}{\partial t} = \frac{\partial u}{\partial t} + \nu\frac{\partial^2 \bar{u}}{\partial z^2} \tag{28}$$

$$\frac{\partial \bar{v}}{\partial t} = \frac{\partial v}{\partial t} + \nu\frac{\partial^2 \bar{v}}{\partial z^2} \tag{29}$$

and the boundary conditions are

$$\bar{u} = \bar{v} = 0 \qquad z = D/2 \tag{30}$$

$$\bar{u}(r,\Phi,z,t) = u(r,\Phi,t) \tag{31a}$$

$$\bar{v}(r,\Phi,z,t) = v(r,\Phi,t) \tag{31b}$$

$$\frac{D/2-z}{\delta} \to \infty \tag{31c}$$

By following the same procedure as was done for the boundary-layer flow over the side wall, the solutions of $\bar{u}$ and $\bar{v}$ are

$$\bar{u} = u - a\left[\frac{(R/r)^2-1}{(R/R_1)^2-1}\right] e^{-\sqrt{\frac{(\sigma-1)\Omega}{2\nu}}(D/2-z)} \times Re\left\{(\dot{\zeta} - i\Omega\zeta)e^{-i\left[\lambda+\sqrt{\frac{(\sigma-1)\Omega}{2\nu}}(D/2-z)\right]}\right\} \tag{32}$$

$$\bar{v} = v - a\left[\frac{(R/r)^2+1}{(R/R_1)^2-1}\right] e^{-\sqrt{\frac{(\sigma-1)\Omega}{2\nu}}(D/2-z)} \times Re\left\{(\dot{\zeta} - i\Omega\zeta)ie^{-i\left[\lambda+\sqrt{\frac{(\sigma-1)\Omega}{2\nu}}(D/2-z)\right]}\right\} \tag{33}$$

Similarly, the shearing force f_T in the r,Φ,z system on the inner top surface of the ring can be obtained by integrating the surface shear stresses $\bar{\tau}_{zr}$ and $\bar{\tau}_{z\Phi}$ over the average area covered by the fluid as

$$f_T = -\int_0^{2\pi}\int_{R_1}^{R}\left[\left(\bar{\tau}_{zr}|_{z=D/2}\right)e_r + \left(\bar{\tau}_{z\Phi}|_{z=D/2}\right)e_\Phi\right] r\,dr\,d\Phi \tag{34}$$

Let $(\bar{f}_X,\bar{f}_Y)$ be the coordinate components of f_T along X,Y axes and denote $f_2 = \bar{f}_X + i\bar{f}_Y$. Then

$$f_2 = -\pi\mu aR_1^2\chi(\dot{\zeta} - i\Omega\zeta + i\dot{\zeta} + \Omega\zeta) \tag{35}$$

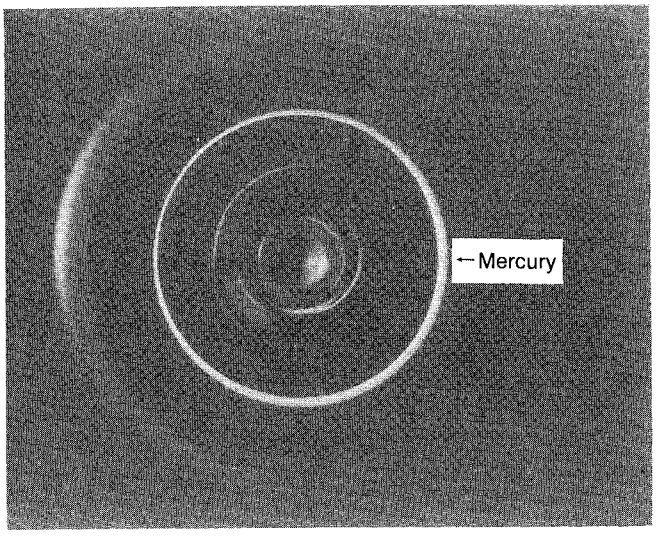

Fig. 3 Snapshot of the mercury in the ring.

The shearing force on the bottom surface ($z = -D/2$) of the ring is the same as that on the top surface due to the symmetric structure of the flow.

Analysis of Gyroscopic System

Figure 3 is a snapshot of the shape of the mercury in the ring when the rotor spinning at a rate of 125 Hz is driven into motion with small nutation angle by a single pulse of magnetic torque. This actual shape does not look like a concentric annulus but an approximate eccentric annulus. The farther from the angular momentum vector of the gyroscope $\boldsymbol{h}$ the cross-section of the eccentric annulus is, the thicker is the thickness of the annulus at that cross section because of the centrifugal effect of precession. Being motivated by that, an eccentric annulus is adopted here to model approximately the shape of the mercury. In other words, the deformation of the mercury is determined by the movement of the inner circle of the eccentric annulus. Referring to Fig. 1, point o'' is the center of the inner circle of the eccentric annulus and is offset a distance s to the point o'. The coordinate system u,v,z is fixed on the mercury with the u axis passing through its mass center. The angular displacement β of the mercury relative to the rotor is measured from the x axis to u axis. The radius of the inner circle of the eccentric annulus is R_1. The mass of the mercury is m_2. The mass of the fictitious mercury that fills the eccentric cylindrical space bordered by the inner surface of the mercury is m_1, i.e., $m_1 = \rho\pi R_1^2 D$ and $m_1 + m_2 = \rho\pi R^2 D$. Based on the fundamental concept that the fluid must form a concentric annulus if the rotor spins purely at a constant speed, we predict that the variable s will tend to zero as the nutation angle approaches zero to account for the fadeout of the centrifugal effect of precession. In order to simplify the analysis, the motion of the center of mass of the mercury is considered instead of that of all the individual particles of the mercury.

The Euler parameters $\boldsymbol{p} = (e_0,e_1,e_2,e_3)^T$, which may be used to form a quaternion,[10,11] are used here instead of Eulerian angles to describe the orientation of the rotor. The quasicoordinates, i.e., the components of angular velocity of the rotor, as well as s and β, are chosen as dependent variables of the equations of motion in order to reduce the numbers of governing equations. The transformation matrix A from $o'xyz$ to $OXYZ$ can be expressed as the product of two 3×4 matrices[12] as

$$\boldsymbol{A} = \boldsymbol{E}\boldsymbol{G}^T \tag{36}$$

where

$$\boldsymbol{E} = \begin{bmatrix} -e_1 & e_0 & -e_3 & e_2 \\ -e_2 & e_3 & e_0 & -e_1 \\ -e_3 & -e_2 & e_1 & e_0 \end{bmatrix}$$

$$\boldsymbol{G} = \begin{bmatrix} -e_1 & e_0 & e_3 & -e_2 \\ -e_2 & -e_3 & e_0 & e_1 \\ -e_3 & e_2 & -e_1 & e_0 \end{bmatrix}$$

The relation of the angular velocity of the rotor in the x,y,z system to the rate of Euler parameters is given by

$$\omega = (\omega_x, \omega_y, \omega_z)^T = 2\boldsymbol{G}\dot{\boldsymbol{p}} = -2\boldsymbol{G}\dot{\boldsymbol{p}} \tag{37}$$

From the point of view of computational efficiency, it is an advantage to use Euler parameters rather than Euler angles because the elements of the transformation matrix and the elements of the matrix that relate the angular velocity to the derivatives of Euler angles are in the form of trigonometric functions if Euler angles are used, but they are linear or quadratic functions of $\boldsymbol{p}$ as shown in Eqs. (36) and (37) if Euler parameters are used. These four Euler parameters are not independent; they satisfy the following constraint equation

$$\boldsymbol{p}^T\boldsymbol{p} = 1 \tag{38}$$

Equations of Motion

The position vector in the u,v,z system and the absolute velocity in x,y,z system of the mass center of the eccentric annulus are

$$(r_c)_{uvz} = \left(\frac{m_1}{m_2}s, 0, a\right)^T \tag{39}$$

$$(v_c)_{xyz} = \frac{\mathrm{d}\boldsymbol{B}^T}{\mathrm{d}t}(r_c)_{uvz} + \boldsymbol{B}^T\frac{\mathrm{d}(r_c)_{uvz}}{\mathrm{d}t} + \omega \times \boldsymbol{B}^T(r_c)_{uvz} \tag{40}$$

respectively. The inertia matrix of the eccentric annulus $\boldsymbol{I}_m$ about its mass center in the u,v,z system is

$$\boldsymbol{I}_m = \mathrm{diag}(I_1,I_2,I_3)_{uvz} \tag{41}$$

where

$$I_1 = \tfrac{1}{4}(m_1 + m_2)R^2 - \tfrac{1}{4}m_1R_1^2$$

$$I_2 = I_1 - \frac{m_1}{m_2}(m_1 + m_2)s^2$$

$$I_3 = 2I_1 - \frac{m_1}{m_2}(m_1 + m_2)s^2$$

$\boldsymbol{I}_m$ depends on the variable s, and so it is time-varying implicitly. The kinetic energy of the mercury T_m is given by

$$T_m = \tfrac{1}{2}[\omega_x, \omega_y, \omega_z + \dot{\beta}]^T\boldsymbol{B}^T\boldsymbol{I}_m\boldsymbol{B}[\omega_x, \omega_y, \omega_z + \dot{\beta}] + (m_2/2)(v_c)_{xyz} \cdot (v_c)_{xyz} \tag{42}$$

The kinetic energy of the rotor T_r is

$$T_r = \tfrac{1}{2}\omega^T\boldsymbol{I}_r\omega$$

where

$$\boldsymbol{I}_r = \mathrm{diag}(I,I,J)_{xyz}$$

I and J are the spin and transverse moments of inertia of the rotor, respectively. The Lagrangian of the gyroscope is $L = T_m + T_r - V_m$. Since the fluid in general does not have strain energy like elastic bodies, the potential energy V_m of the mercury comes only from the gravitational potential, as the following

$$V_m = -m_2 \boldsymbol{g}^T \boldsymbol{A} \boldsymbol{B}^T (\boldsymbol{r}_c)_{uvz}$$

where $\boldsymbol{g} = (g_X, g_Y, g_Z)^T$ is the gravity with components parallel to X, Y, Z. The governing equations derived by using the method of Lagrange multipliers have an additional unknown, the Lagrange multiplier, due to the constraint equation (38) besides the variables p, s, and β. If the arguments $\dot{p}$ in $L(p, s, \beta, \dot{p}, \dot{s}, \dot{\beta})$ are replaced by the quasicoordinates ω, the governing equations of the gyroscope for the Lagrangian $\bar{L}(p, s, \beta, \omega, \dot{s}, \dot{\beta})$ have the form[4]

$$\frac{d}{dt}\left(\frac{\partial \bar{L}}{\partial \omega}\right) + \tilde{\omega}\left(\frac{\partial \bar{L}}{\partial \omega}\right) - \frac{1}{2}\boldsymbol{G}\left(\frac{\partial \bar{L}}{\partial p}\right) = \boldsymbol{m} \tag{43}$$

$$\frac{d}{dt}\left(\frac{\partial \bar{L}}{\partial \dot{\beta}}\right) - \left(\frac{\partial \bar{L}}{\partial \beta}\right) = Q_\beta \tag{44}$$

$$\frac{d}{dt}\left(\frac{\partial \bar{L}}{\partial \dot{s}}\right) - \left(\frac{\partial \bar{L}}{\partial s}\right) = Q_s \tag{45}$$

$$\dot{p} = \tfrac{1}{2}\boldsymbol{G}^T \omega \tag{46}$$

where

$$\tilde{\omega} = \begin{pmatrix} 0 & -\omega_z & \omega_y \\ \omega_z & 0 & -\omega_x \\ -\omega_y & \omega_x & 0 \end{pmatrix}$$

The vector $\boldsymbol{m}$ is the generalized torques produced by the gravitational force of the mercury. On the assumptions that the spin rate of the rotor is high enough and the mass of the mercury is sufficiently small, the gravitational effect of the mercury is neglected, i.e., $V_m = 0$ in $\bar{L}$ and $\boldsymbol{m} = 0$ in Eq. (43) because it does not have significant influence on the behavior of the nutation angle.[4] Thus, the Lagrangian $\bar{L}$ does not contain the arguments p, and Eqs. (43–45) can be solved independently without coupling with Eq. (46). The nutation angle θ, however, is not one of the dependent variables of the governing equation, but it can be obtained by solving the following equation:

$$\tan\theta = \frac{h_z}{h_t} \tag{47}$$

where h_z and h_t are the spin and transverse components of the angular momentum of the gyroscope about the point o in the x, y, z system, respectively.

Generalized Forces

Before proceeding to derive the generalized forces Q_β and Q_s in Eqs. (44) and (45), we have to find the relation between wave variables (ζ and η) and the variables s and β. Thus, the shearing forces in terms of wave variables and their time derivatives can be converted in terms of s, $\dot{s}$, β, and $\dot{\beta}$. Referring to Fig. 1, the vector r with the angle α_1 measured from the u axis is the position vector of an arbitrary fluid particle on the free surface. From the sinusoidal law we have

$$\frac{\sin(\pi - \alpha_1)}{R_1} = \frac{\sin\alpha_2}{s} = \frac{\sin\alpha_3}{r} \tag{48}$$

and so

$$r = \frac{R_1}{\sin\alpha_1}\sin\alpha_3 = R_1\cos\alpha_2 - s\cos\alpha_1$$

$$= R_1\sqrt{1 - \left(\frac{s}{R_1}\sin\alpha_1\right)^2} - s\cos\alpha_1 \tag{49}$$

Because of the assumption of small-amplitude wave, the value of s/R_1 is very small. Hence, Eq. (49) can be simplified as

$$r = R_1 - s\cos\alpha_1 \tag{50}$$

Substituting $\Phi = \beta + \alpha_1$ into Eq. (50) and comparing it with the equation $r = R_1 + r_1(\Phi, t)$, the amplitude of the surface wave of the mercury is given as

$$r_1(\Phi, t) = -s\cos(\Phi - \beta) \tag{51}$$

We rewrite Eq. (51) in the following form

$$r_1(\Phi, t) = -s\cos(\Omega t + \Phi - \Omega t - \beta)$$

$$= -s[\cos\lambda\cos(\Omega t + \beta) + \sin\lambda\sin(\Omega t + \beta)] \tag{52}$$

where $\lambda \approx \Omega t + \Phi$, since $\omega_z = \dot{\phi} + \dot{\psi} \approx \Omega$. Equation (52) is equivalent to the following equation

$$r_1(\Phi, t) = aRe\left\{\left[-\frac{s}{a}\cos(\Omega t + \beta) - i\frac{s}{a}\sin(\Omega t + \beta)\right]e^{-i\lambda}\right\} \tag{53}$$

Comparing Eq. (53) with Eq. (14), we have

$$\xi(\Phi, t) = -\frac{s}{a}\cos(\Omega t + \beta) \tag{54a}$$

$$\eta(\Phi, t) = -\frac{s}{a}\sin(\Omega t + \beta) \tag{54b}$$

Let $\boldsymbol{f} = (F_X, F_Y, F_Z)^T$ be the X, Y, Z coordinate components of the net shearing force acting on the rotor by the mercury. It is the vector sum of the shearing forces on the side wall, the top surface, and the bottom surface of the ring. From Eqs. (27) and (35), we have

$$F_X = -c(\dot{\xi} - \dot{\eta} + \Omega\eta + \Omega\xi) \tag{55a}$$

$$F_Y = -c(\dot{\eta} + \dot{\xi} + \Omega\eta - \Omega\xi) \tag{55b}$$

where

$$c = \mu a \pi \chi\left[DR\left(\frac{R^2 + R_1^2}{R^2 - R_1^2}\right) + 2R_1^2\right]$$

The substitution of Eqs. (54) and its time derivative into Eqs. (55) yields

$$F_X = -c\left\{-\frac{\dot{s}}{a}[\cos(\Omega t + \beta) - \sin(\Omega t + \beta)] + \frac{s\dot{\beta}}{a}[\sin(\Omega t + \beta) + \cos(\Omega t + \beta)]\right\} \tag{56a}$$

$$F_Y = -c\left\{-\frac{\dot{s}}{a}[\cos(\Omega t + \beta) + \sin(\Omega t + \beta)] + \frac{s\dot{\beta}}{a}[\sin(\Omega t + \beta) - \cos(\Omega t + \beta)]\right\} \tag{56b}$$

The generalized forces Q_β and Q_s can be obtained from the principle of virtual work. Because the mercury has two more degrees of freedom represented by the variables s and β than the rotor, the shearing force between them is an internal force that will produce nonvanishing virtual work. Let δW denote the net virtual work produced by the shearing force acting on the mercury by the rotor in the direction of the virtual displacement of the center of mass of the mercury relative to the rotor, that is,

$$\delta W = -f \cdot \delta r_{oc} = -\left(f \cdot \frac{\partial r_{oc}}{\partial \beta}\,\delta\beta + f \cdot \frac{\partial r_{oc}}{\partial s}\,\delta s\right) \tag{57}$$

where $-f$ is the reaction force exerted by the rotor on the mercury, r_{oc} is the position vector of the point o'' with respect to the point o'. With components along the X, Y, Z axes, r_{oc} is

$$r_{oc} = AB^T\left(\frac{m_1}{m_2}s, 0, 0\right)^T_{uvz}$$

and so

$$\frac{\partial r_{oc}}{\partial \beta} = A\frac{\partial B^T}{\partial \beta}\left(\frac{m_1}{m_2}s, 0, 0\right)^T_{uvz}$$

$$= \left[-\frac{m_1}{m_2}s\sin(\Omega t+\beta), \frac{m_1}{m_2}s\cos(\Omega t+\beta),\right.$$

$$\left.-\frac{m_1}{m_2}s\theta\cos(\Omega t+\beta)\right]^T \tag{58}$$

Similarly,

$$\frac{\partial r_{oc}}{\partial s} = \left[\frac{m_1}{m_2}\cos(\Omega t+\beta), \frac{m_1}{m_2}\sin(\Omega t+\beta),\right.$$

$$\left.-\frac{m_1}{m_2}\theta\sin(\Omega t+\beta)\right]^T \tag{59}$$

The substitution of Eqs. (56), (58), and (59) into Eq. (57) yields

$$\delta W = -\frac{m_1}{m_2}sc\left(\frac{\dot{s}}{a}+\frac{s\dot{\beta}}{a}\right)\delta\beta - \frac{m_1}{m_2}c\left(\frac{\dot{s}}{a}-\frac{s\dot{\beta}}{a}\right)\delta s \tag{60}$$

From the definition of generalized forces, we have

$$Q_\beta = -\frac{m_1}{m_2}sc\left(\frac{\dot{s}}{a}+\frac{s\dot{\beta}}{a}\right) \tag{61a}$$

$$Q_s = -\frac{m_1}{m_2}c\left(\frac{\dot{s}}{a}-\frac{s\dot{\beta}}{a}\right) \tag{61b}$$

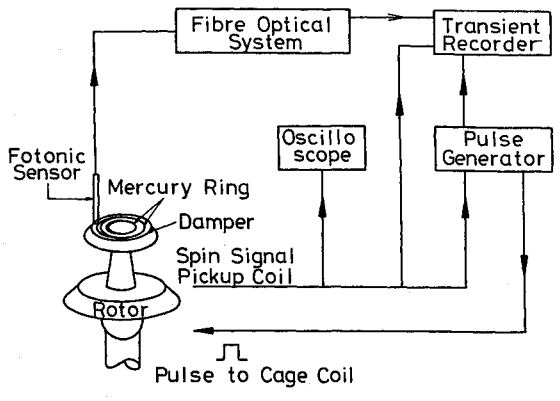

Fig. 4 Diagram of the measuring system.

Experimental Test

An experiment was performed to verify the behavior of the nutation angle of the rotor. The damper used here has double rings inside. The diagram of the measuring system is shown in Fig. 4. A small coil was placed beside the rotor-driving coil to pick up the spin rate of the rotor. This signal was also used to trigger the pulse generator to generate single square wave. This pulse was applied to the caging coil to produce a magnetic torque to the rotor so that the rotor was in motion with small nutation angle. A fiber optical displacement system[13] was used to measure the response of the rotor. The response recorded is a combination of nutation and precession of the rotor.

Results and Discussion

The nonlinear governing equations [Eqs. (43–45)] (see the Appendix) were solved by numerical integration. First, we consider the specific example for which the damper has a single ring inside, $I = 197.35$ g – cm^2, $J = 279.52$ g – cm^2, $\Omega = 125$ Hz, $a = 2.427$ cm, $D = 0.078$ cm, $\Delta R = R - R_0 = 0.14$ cm, and $R = 1.015$ cm. The kinematic viscosity ν of mercury is 0.00117 cm^2/s. The amount of mercury is $\tilde{h}/\Delta R = 0.25$, where $\tilde{h} = R - R_1$. Figure 5 is the time history of the nutation angle θ. Using the least squares method to fit the θ curve for the function $A_0 e^{-t/\tau}$, we obtain the decay time constant $\tau = 0.229$ s. The feature that the nutation angle decays exponentially to zero is the relative merit of the fluid mode over the nutation and spin synchronous modes for which there exists a residual nutation angle. Figure 6 shows that the variable s

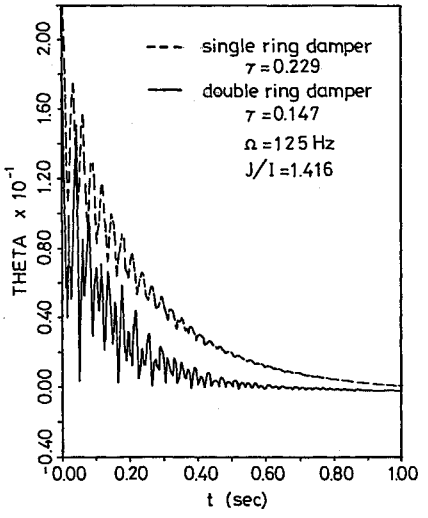

Fig. 5 Time history of θ.

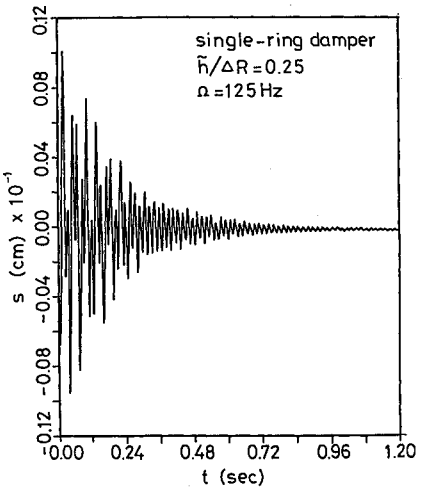

Fig. 6 Time history of s.

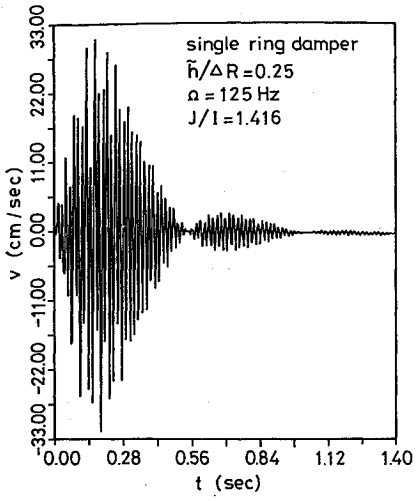

Fig. 7 Tangential velocity of the mercury flow at $r = R_1$, $\Phi = 0$ deg.

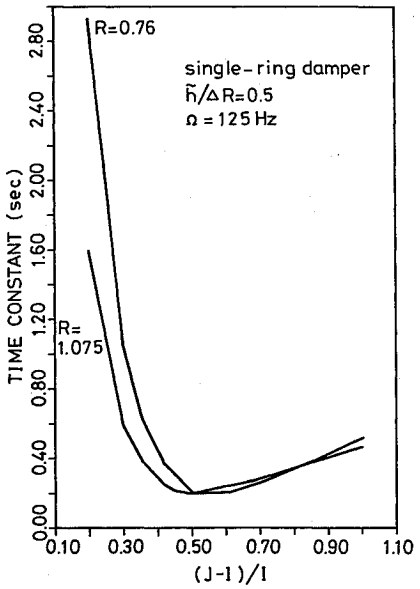

Fig. 8 The τ vs $(J/I - 1)$.

approaches zero as θ tends to zero. This means that the eccentric mercury becomes concentric, finally. Therefore, the phenomenon of mass imbalance due to the crescent mercury in nutation and spin synchronous modes does not appear in the fluid mode. From Eqs. (12b) and (53), the tangential velocity of the mercury flow outside the boundary layer is

$$v(r,\Phi,t) = -a\left[\frac{(R/r)^2+1}{(R/R_1)^2-1}\right] \times Re\{-\dot{\xi}\sin(\Omega t+\Phi)+\dot{\eta}\cos(\Omega t+\Phi) - \Omega[\xi\cos(\Omega t+\Phi)+\eta\sin(\Omega t+\Phi)]\} \quad (62)$$

The time history of v at the point $r = R_1$, $\Phi = 0$ deg is shown in Fig. 7, and it also approaches zero as θ goes to 0 deg. All of these imply that the mercury will synchronize with the rotor finally at $\theta = 0$ deg. The beat phenomenon in v does not appear in θ. This can be interpreted from the mathematical viewpoint in the way that the dependent variables of governing equations do not have beat phenomenon such as s in Fig. 6, v is evaluated from Eq. (62) and the wave variables ξ and η, which appear in Eq. (62), are related to the dependent variables by Eq. (54); it is that one of the harmonic solutions of dependent variables has the value of frequency close to Ω so that the term $s \times \cos(\Omega t + \beta)$ in Eq. (54) has beat phenomenon. θ is found from Eq. (47) and it does not contain those terms that cause beat phenomenon as v does.

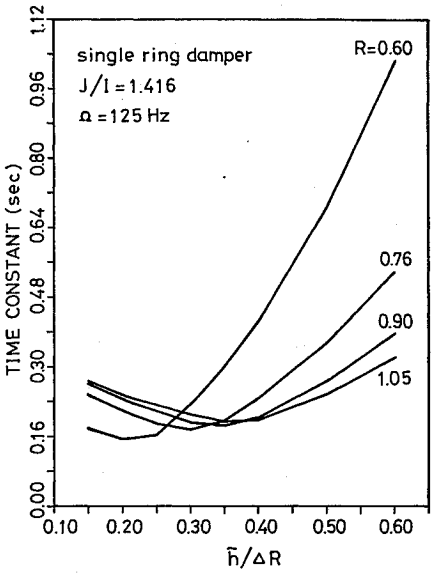

Fig. 9 The τ vs $\tilde{h}/\Delta R$.

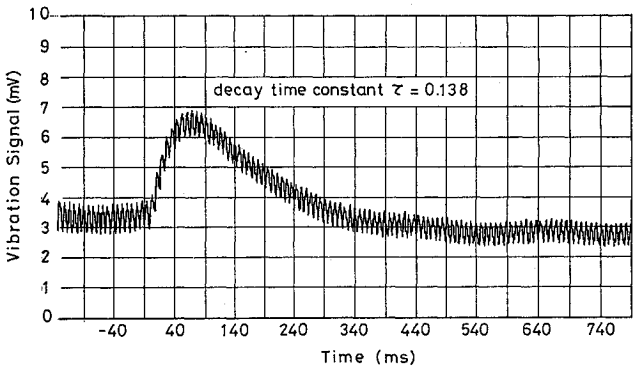

Fig. 10 Vibration signal of nutation and precession: $\tilde{h}_i/\Delta R = 0.5$; $\tilde{h}_o/\Delta R = 0.25$.

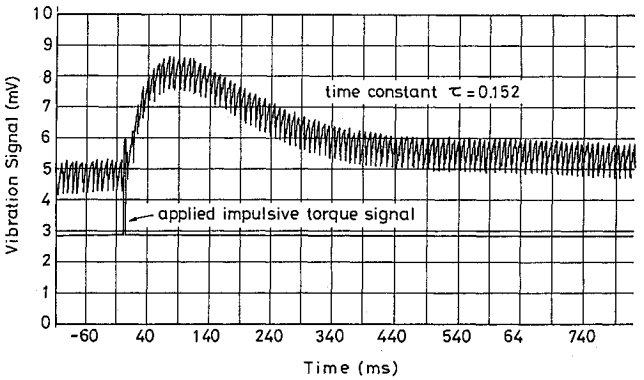

Fig. 11 Vibration signal of nutation and precession: $\tilde{h}_i/\Delta R = \tilde{h}_o/\Delta R = 0.25$.

Figure 8 shows that the ratio J/I has significant influence on the decay time constant τ. The optimal value of J/I is about 1.5 for $\tilde{h}/\Delta R = 0.5$ and $\tau \to \infty$ as $J/I \to 1$. Figure 9 shows that τ is a concave function of $h/\Delta R$ for various fixed values of R. The smaller the R is, the less must be the amount of mercury for achieving the least decay time constant. Furthermore, we consider the previous example with double rings damper instead. For this problem, we have two more generalized coordinates that are needed to describe the position of the mass center of the mercury in the second ring. The equations of motion can be derived straightforward in the same manner as those of the gyroscope with single ring damper. The radii of

the inner ring and outer ring are 0.76 and 1.015 cm, respectively. The amounts of mercury that filled the inner and outer ring are $\tilde{h}_i/\Delta R = 0.5$ and $\tilde{h}_o/\Delta R = 0.25$, respectively. The time history of the nutation angle is shown in Fig. 5 and the corresponding decay time constant is $\tau = 0.147$ s. The vibration signal output from the Fotonic sensor and shown in Fig. 10 is the response of nutation and precesion. The harmonic signal with frequency 125 Hz carried on the exponentially decaying envelope is due to the spin of the rotor. The decay time constant by curve-fitting is 0.138 s and a little bit less than the theoretically predicted. Figure 11 is the vibration signal for the other case in which $\tilde{h}_i/\Delta R = \tilde{h}_o/\Delta R = 0.25$. The time constant is $\tau = 0.152$, which is close to the theoretical result $\tau = 0.168$ (as it can be seen in Fig. 13). The closeness between the experimental and theoretical results for the time constant based on the two data points indicates that our modeling is valid, approximately. Hence, based on the equations of motion, the effects of key parameters of the damper on the decay time constant can be analyzed. Values of τ are plotted as a function of $\tilde{h}_o/\Delta R$ at various values of $\tilde{h}_i/\Delta R$ in Fig. 12. Figure 13 shows the curves of τ vs $\tilde{h}_i/\Delta R$ at various values of $\tilde{h}_o/\Delta R$. All of the curves in Figs. 12 and 13 start from $\tilde{h}_j/\Delta R = 0.2$, whether $j = i$ or $j = o$, because the mercury fails to form a continuous annulus and is out of the application of the eccentric annulus modeling when the amount of mercury is less than that value.

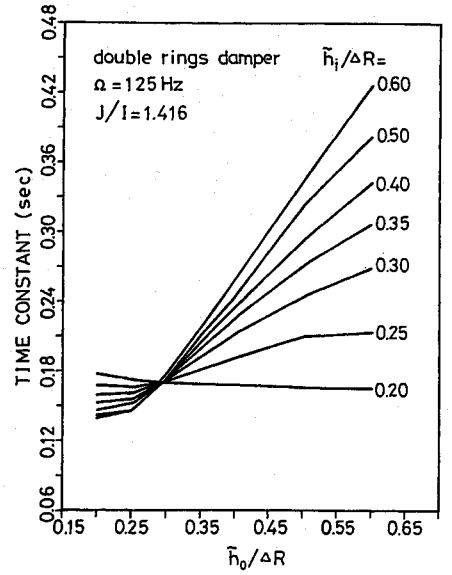

Fig. 12 The τ vs $\tilde{h}_o/\Delta R$ at various values of $\tilde{h}_i/\Delta R$.

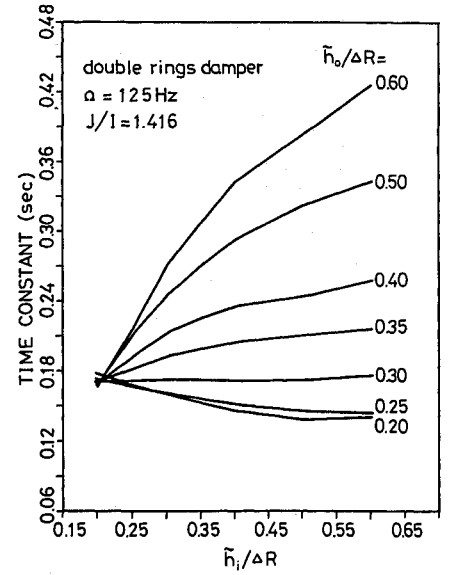

Fig. 13 The τ vs $\tilde{h}_i/\Delta R$ at various values of $\tilde{h}_o/\Delta R$.

By observing the trend of the curves in Figs. 12 and 13, we conclude that the minimum decay time constant will occur in the case where the angle of fill is 180 deg for the inner ring and about 80 deg for the outer ring. This result cannot be obtained by direct deduction from the trend of the single ring damper shown in Fig. 9. It is worth mentioning that the double ring damper does not reduce the minimum decay time constant to one half of that of the single ring damper. This means that the decay time constant is not inversely proportional to the number of the rings inside the damper.

The advantage of using quasicoordinates as dependent variables is that the governing equations will result in seven first-order ordinary differential equations. Contrarily, if the Eulerian angles are used instead, the governing equations will result in 10 first-order ordinary differential equations. This will increase the degree of difficulty in analyzing the stability or bifurcation problem by analytical methods. A related paper studies the stability about a equilibrium point of the same problem by the perturbation technique.[14]

Conclusion

In this paper, an eccentric annulus is proposed to model approximately the actual shape of the mercury in the ring damper. New coupled equations of motion of the rotor and the mercury are derived for the fluid mode problem and in the form of ordinary differential equations rather than partial differential equations. The numerical results show that the nutation angle indeed decays to zero and, in the meanwhile, the mercury deforms from the shape like an eccentric annulus to that like a concentric annulus. This is the relative merit of the fluid mode over the nutation and spin synchronous modes in which there exist the phenomenon of residual nutation angle. The agreement between the experimental result and the theoretical prediction on the decay time constant based on two data points reveals that our mathematical modeling is approximately valid. The ratio of the spin moment of inertia of the rotor to its transverse moment of inertia has significant influence on the decay time constant. For our illustrated examples, the minimum decay time constant of the double ring damper is less than that of the single ring damper by 36% and occurs in the case where the angle of fill is 180 deg for the inner ring and about 80 deg for the outer ring. The approach can be extended to treat multiple ring dampers without difficulty.

Appendix

Equations (52), (53), and (54) are rearranged in the form as

$$D_{5\times 5}\dot{y} = f(y,t)$$

where $y = (\omega_z, \omega_y, \omega_z, \dot{\beta}, \dot{s})^T$ and the nonzero elements of the matrix D are

$$D_{11} = I + I_1 \cos^2\beta + \left(I_2 + \frac{m_1^2}{m_2} s^2\right) \sin^2\beta + m_2 a^2$$

$$D_{12} = (I_1 - I_2) \cos\beta \sin\beta - \frac{m_1^2}{m_2} s^2 \cos^2\beta \sin\beta$$

$$D_{13} = D_{14} = -m_1 as \cos\beta$$

$$D_{15} = -m_1 a \sin\beta, \qquad D_{21} = D_{12}$$

$$D_{22} = I + I_1 \sin^2\beta + \left(I_2 + \frac{m_1^2}{m_2} s^2\right) \cos^2\beta + m_2 a^2$$

$$D_{23} = D_{24} = -m_1 as \sin\beta, \qquad D_{25} = m_1 a \cos\beta$$

$$D_{31} = D_{13}, \qquad D_{32} = D_{23}$$

$$D_{33} = J + I_3 + \frac{m_1^2}{m_2} s^2, \qquad D_{34} = I_3 + \frac{m_1^2}{m_2} s^2$$

$$D_{41} = D_{14}, \qquad D_{42} = D_{24}$$

$$D_{43} = D_{34}, \qquad D_{44} = I_3 + \frac{m_1^2}{m_2} s^2$$

$$D_{51} = D_{15}, \qquad D_{52} = D_{25}, \qquad D_{55} = \frac{m_1^2}{m_2}$$

The elements of the vector f are as follows:

$$\begin{aligned} f_1 = {} & [(I_1' - I_2') \sin\beta \cos\beta]\omega_x\omega_z + I_4' \cos\beta\omega_x\omega_y \\ & - (I_3' + J - I - I_1' \sin^2\beta - I_2' \cos^2\beta)\omega_y\omega_z - I_4' \sin\beta\omega_z^2 \\ & + I_4' \sin\beta\omega_y^2 + 2(I_1' - I_2') \sin\beta \cos\beta\dot{\beta}\omega_x \\ & - [(I_1' - I_2') (\cos^2\beta - \sin^2\beta) + I_3'] \dot{\beta}\omega_y \\ & - 2I_4' \sin\beta\dot{\beta}\omega_z - I_4' \sin\beta\dot{\beta}^2 + m_1 gs \sin\beta(e_1^2 - e_0^2 - e_3^2 + e_2^2) \\ & + 2m_2 ga(e_2e_3 + e_0e_1) + 2m_1 s \sin^2\beta\dot{s}\omega_x \\ & - m_1 s \sin 2\beta\dot{s}\omega_y + 2m_1 a \cos\beta\dot{s}\omega_z + 2m_1 a \cos\beta\dot{s}\dot{\beta} \end{aligned}$$

$$\begin{aligned} f_2 = {} & - I_4' \sin\beta\omega_z\omega_y - (I_1' - I_2') \sin\beta \cos\beta\omega_y\omega_z \\ & + (-I + J + I_3' - I_1' \cos^2\beta - I_2' \sin^2\beta)\omega_x\omega_z - I_4' \cos\beta\omega_x^2 \\ & + I_4' \cos\beta\omega_z^2 + [I_3' - (I_1 - I_2')(\cos^2\beta - \sin^2\beta)] \dot{\beta}\omega_x \\ & - 2(I_1' - I_2') \sin\beta \cos\beta\dot{\beta}\omega_y + 2I_4' \cos\beta\dot{\beta}\omega_z \\ & + I_4' \cos\beta\dot{\beta}^2 + m_1 gs \cos\beta(e_0^2 - e_1^2 - e_2^2 + e_3^2) \\ & + 2m_2 ga(e_0e_2 - e_1e_3) - m_1 s \sin 2\beta\dot{s}\omega_x + 2m_1 s \cos^2\beta\dot{s}\omega_y \\ & + 2m_1 a \sin\beta\dot{s}\omega_z + 2m_1 a \sin\beta\dot{s}\dot{\beta} \end{aligned}$$

$$\begin{aligned} f_3 = {} & I_4' \sin\beta\omega_x\omega_z - I_4' \cos\beta\omega_y\omega_z \\ & + (I_1' - I_2')(\cos^2\beta - \sin^2\beta)\omega_x\omega_y + 2m_1 s\dot{s}(\omega_z + \dot{\beta}) \\ & - 2m_1 gs \cos\beta(e_2e_3 + e_0e_1) - (I_1' - I_2') \sin\beta \cos\beta(\omega_x^2 - \omega_y^2) \\ & + 2m_1 gs \sin\beta(e_1e_3 - e_0e_2) \end{aligned}$$

$$\begin{aligned} f_4 = {} & I_4' \sin\beta\omega_x\omega_z - I_4' \cos\beta\omega_y\omega_z \\ & + (I_1' - I_2')(\cos^2\beta - \sin^2\beta)\omega_x\omega_y + 2m_1 s\dot{s}(\omega_z + \dot{\beta}) \\ & - 2m_1 gs \cos\beta(e_2e_3 + e_0e_1) - (I_1' - I_2') \sin\beta \cos\beta(\omega_x^2 - \omega_y^2) \\ & + 2m_1 gs \sin\beta(e_1e_3 - e_0e_2) + Q_\beta \end{aligned}$$

$$\begin{aligned} f_5 = {} & - m_1 a \cos\beta\omega_x\omega_z - m_1 a \sin\beta\omega_y\omega_z \\ & - 2m_1 g \sin\beta(e_2e_3 + e_0e_1) - m_1 s[(-\omega_x \sin\beta + \omega_y \cos\beta)^2 \\ & + (\omega_z + \dot{\beta})^2] - 2m_1 g \cos\beta(e_1e_3 - e_0e_2) + Q_s \end{aligned}$$

where I_1', I_2', I_3', and I_4' are

$$I_1' = I_1 + m_2 a^2, \qquad I_2' = I_1 - m_1 s^2 + m_2 a^2$$

$$I_3' = 2I_1 - m_1 s^2, \qquad I_4' = m_1 sa$$

and they are the nonzero elements of the matrix I_m', which is the inertia matrix of the eccentric annulus about the point o in the u,v,z coordinate system and has the form

$$I_m' = \begin{bmatrix} I_1' & 0 & -I_4' \\ 0 & I_2' & 0 \\ -I_4' & 0 & I_3' \end{bmatrix}$$

References

[1]Cartwright, W. F., Massingill, E. C., and Trueblood, R. O., "Circular Constraint Nutation Damper," *AIAA Journal,* Vol. 1, No. 6, 1963, pp. 1375–1380.

[2]Alfriend, K. T., "Partially Filled Viscous Ring Nutation Damper," *Journal of Spacecraft and Rockets,* Vol. 11, No. 7, 1974, pp. 456–462.

[3]Alfriend, K. T., and Spencer, T. M., "Comparison of Filled and Partially Filled Nutation Damper," *Journal of Astronautical Sciences,* Vol. 31, No. 2, 1983, pp. 198–202.

[4]Chang, C. O., and Chou, C. S., "Dynamic Analysis and Optimal Design of the Viscous Ring Nutation Damper for a Freely Precessing Gyroscope," *Proceedings of the 29th AIAA/ASME/ASCE/AHS Structures, Structural Dynamics, and Materials Conference,* AIAA, Washington, DC, 1988, pp. 411–419.

[5]Bhuta, P. G., and Koval, L. R., "A Viscous Ring Damper for a Freely Precessing Satellite," *International Journal of Mechanical Science,* Vol. 8, 1966, pp. 383–395.

[6]Carrier, G. F., and Miles, J. W., "On the Annular Damper for a Freely Precessing Gyroscope," *Journal of Applied Mechanics,* Vol. 30, 1960, pp. 237–240.

[7]Miles, J. W., "On the Annular Damper for a Freely Precessing Gyroscope—II," *Journal of Applied Mechanics,* Vol. 30, 1963, pp. 189–192.

[8]Fitzgibbon, D. P., and Smith, W. E., "Second Status Report on the Experimental Evaluation of Passive Systems for Damping Wobble of a Free Spinning Rigid Body," Space Technology Laboratories, Inc., Los Angeles, CA, 1961.

[9]Meirovitch, L., *Methods of Analytical Dynamics,* McGraw-Hill, New York, 1970, pp. 140–146.

[10]Whittaker, E. T., *A Treatise on the Analytical Dynamics of Particles and Rigid Bodies,* 4th ed., Cambridge University Press, Cambridge, England, UK, 1937.

[11]Goldstein, H., *Classical Mechanics,* 2nd ed., Addison Wesley, Reading, MA, 1980, pp. 148–155.

[12]Nikravesh, P. E., *Computer-Aided Analysis of Mechanical Systems,* Prentice-Hall, Englewood Cliffs, NJ, 1988, pp. 166–176.

[13]Cook, R. O., and Hamm, C. W., "Fiber Optic Lever Displacement Transducer," *Applied Optics,* Vol. 18, No. 19, 1979, pp. 320–324.

[14]Chang, C. O., and Chou, C. S., "Dynamic Stability Analysis of a Freely Precessing Gyroscope Carrying Mercury Ring Damper," *Journal of Sound and Vibration*, Vol. 144, No. 1, 1991.